

Development and clinical validation of a hybrid method for semiautomated left ventricle endocardial and epicardial boundary extraction on cine-magnetic resonance images

Mahammed Messadi,^a Abdelhafid Bessaid,^a Denis Mariano-Goulart,^b and Fayçal Ben Bouallègue^{b,*}

^aAboubakr Belkaid University, Biomedical Engineering Department, Tlemcen, Algeria

^bMontpellier University Hospital, Nuclear Medicine Department, Montpellier, France

Abstract. We describe a hybrid method for left ventricle (LV) endocardial and epicardial segmentation on cardiac magnetic resonance (CMR) images requiring minimal operator intervention. Endocardium extraction results from the union of three independent estimations based on adaptive thresholding, region growing, and active contour with Chan—Vese energy function. Epicardium segmentation relies on conditional morphological dilation of the endocardial mask followed by active contour optimization. The proposed method was first evaluated using an open access database of 18 CMR for which expert manual contouring was available. The method was further validated on a retrospective cohort of 29 patients, who underwent CMR with expert manual segmentation. Regarding the open access database, similarity (Dice index) between hybrid and expert segmentations was good for end-diastolic (ED) endocardium (0.92), end-systolic (ES) endocardium (0.88), and ED epicardium (0.92). As for derived LV parameters, concordance (Lin's coefficient) was good for ED volume (0.91), ES volume (0.93), ejection fraction (EF; 0.89), and fair for myocardial mass (MM; 0.74). Regarding the retrospective patient study, concordance between expert and hybrid estimations was excellent for ED volume (0.95), ES volume (0.96), good for EF (0.86), and fair for MM (0.71). Hybrid segmentation resulted in small biases (−6 mL for ED volume, +4 mL for ES volume, −6% for EF, and −6 g for MM) with little clinical relevance and acceptable for routine practice. The quickness and robustness of the proposed hybrid method and its ability to provide LV volumes, functions, and masses highly concordant with those given by expert segmentation support its pertinence for routine clinical use. © 2018 Society of Photo-Optical Instrumentation Engineers (SPIE) [DOI: 10.1117/1.JMI.5.2.024002]

Keywords: cardiac magnetic resonance; left ventricle segmentation; endocardium; epicardium.

Paper 17265R received Sep. 10, 2017; accepted for publication Mar. 19, 2018; published online Apr. 11, 2018.

1 Introduction

The estimation of left ventricle (LV) functional parameters, such as end-diastolic volume (EDV), end-systolic volume (ESV), and ejection fraction (EF), requires the segmentation of the LV cavity on short axis (SA) dynamic cardiac magnetic resonance (CMR) images.¹ Assessment of myocardial mass (MM), a crucial parameter in the diagnosis and follow-up of hypertrophic cardiomyopathy, necessitates further delineation of the LV epicardial border. In routine practice, a manual delineation of the endocardial (and eventually epicardial) contours is usually performed, which is known to be highly time consuming and prone to intra- and interobserver variability.^{2,3} The main issues regarding endocardium segmentation relate to gray-level inhomogeneities in the blood flow, the presence of wall irregularities (papillary muscles and trabeculations), partial volume effect in apical slices, noise and motion artifacts associated to heart dynamics. With respect to epicardium delineation, its complexity rises from the presence of several surrounding tissues (fat, lung, and liver) with different intensity profiles and poor contrast with the myocardium. The development of automatic

or semiautomatic LV segmentation methods is therefore an active research focus in the field of medical image processing,^{3,4} and numerous approaches have been reported these last two decades in the literature. Most rely either on image-based methods, such as thresholding^{5,6} or dynamic programming,^{7,8} pixel classification methods, such as Gaussian mixture models⁹ or clustering,^{10,11} or deformable models, such as active contour.^{12,13} These methods imply weak or even no prior assumption regarding object shape or signal distribution. On the other hand, image-based methods usually require operator intervention for initialization of the segmentation process and/or *a posteriori* manual correction, which might be time-consuming and impact reproducibility. Besides, automatic organ segmentation can benefit from the use of a statistical model regarding shape and/or gray levels, to increase its robustness and accuracy. Such methods using strong priors include deformable models,^{14–16} active shape and appearance models,^{17,18} and atlas-guided segmentation.^{19,20} Their main drawback lies in the need to build large training datasets with manually generated segmentations accounting for the considerable variability in shape and intensity of the heart chambers across patients, notably in pathological cases. While most segmentation methods focus on endocardial

*Address all correspondence to: Fayçal Ben Bouallègue, E-mail: fayben@hotmail.com

border delineation for LV volume and function assessment, several algorithms also extend to epicardium segmentation allowing (based on voxel summation and an average value for myocardium density of 1.05 g/mL) to estimate MM.^{17,21–23}

The aim of the present paper is to describe a semiautomated algorithm for LV endocardial and epicardial contour delineation in SA cine-MR images, which requires minimal operator intervention. The proposed method is hybrid in the sense that it combines the results of three distinct segmentation algorithms (adaptive thresholding, active contour, and region growing) in order to optimize LV cavity extraction. LV epicardial boundary was performed starting from the endocardial mask using morphological dilation followed by active contour segmentation. Adaptive thresholding, active contour, and region growing were chosen because they are well-established, computationally efficient techniques that do not imply any prior regarding myocardial shape. They were implemented in a chained and sequential fashion in order to ensure robustness by minimizing operator intervention.

The performance of the method was first assessed using an open access clinically validated cine-MR database. Semiautomated hybrid segmentations were compared with manual expert delineations using Dice overlapping metrics and average perpendicular distance, and in terms of LV functional parameters (EDV, ESV, EF, and MM). Second, the method was evaluated on CMR data of a retrospective cohort from Montpellier University Hospital, France. EDVs and ESVs, EFs, and MMs estimated using the hybrid method were compared to those provided by expert manual CMR.

2 Materials and Methods

2.1 Hybrid Segmentation Algorithm

The proposed technique was developed and run using MATLAB (Math Works, Natick, Massachusetts). LV endocardial contour determination was composed of three segmentation methods which results were combined. The final LV cavity segmentation was defined as the union of the endocardial segmentations provided by the three methods. As a preprocessing step, SA images were contrast-enhanced using morphological opening with a seven-pixel radius structuring element, and then pixel values were resampled using 256 gray levels between 0 and 255. The first method consisted in an adaptive thresholding algorithm, which required manual intervention for region affectation either to LV or background. The second and third methods relied, respectively, on active contour and region growing and were fully automated. They exploited as initial condition the segmentation mask provided by the first method. After endocardium extraction, LV epicardial boundary was estimated starting from the endocardial segmentation mask using morphological dilation with structuring elements of increasing size followed by active contour optimization.

2.1.1 Endocardial boundary—adaptive thresholding

Adaptive thresholding was realized on each SA slice through the following steps:

- Multilevel image thresholding using Otsu’s method²⁴ with an empirically fixed number of levels set to 7. Otsu’s method is a fast algorithm for optimal histogram clustering based on interclass variance maximization.

- Labeling of the connected components.
- Hole-filling of the label image.
- Smoothing of the label image using morphological opening (erosion using as a structuring element a 2 pixel radius disk, then dilation using as structuring element a 4 pixel radius disk).
- Manual selection of the lowest mean intensity region belonging to the LV cavity. This was the only step requiring operator intervention.
- Aggregation to the manually selected region, among those connected to it, of those with higher mean intensity.

2.1.2 Endocardial boundary—active contour

We used the “active contours without edge method” proposed by Chan and Vese.²⁵ It is inspired by the Mumford–Shah model,²⁶ which approximates an image I defined over a bounded domain Ω by a piece-wise smooth function u as the solution of the minimization problem:

$$\operatorname{argmin}_{u,C} \left\{ \mu \operatorname{Length}(C) + \sigma \int_{\Omega} [I(x) - u(x)]^2 dx + \int_{\Omega_C} |\nabla u(x)|^2 dx \right\}, \quad (1)$$

where C is an edge set curve where u is allowed to be discontinuous, and μ and σ are weighting constants. The Mumford–Shah approximation suggests selecting this edge set C as the segmentation boundary. Compared to the Mumford–Shah model, the key differences in the Chan–Vese model are an additional term penalizing the enclosed area and a further simplification that u is piecewise constant and allowed to have only two values:

$$u(x) = \begin{cases} c_1 & \text{where } x \text{ is inside } C \\ c_2 & \text{where } x \text{ outside } C \end{cases}, \quad (2)$$

where C is the boundary of a closed set and c_1, c_2 are the values of u , respectively, inside and outside of C . The Chan–Vese method is to find among all u of this form the one that best approximates I :

$$\operatorname{argmin}_{c_1, c_2, C} \left\{ \mu \operatorname{Length}(C) + \nu \operatorname{Area}[\operatorname{inside}(C)] + \sigma_1 \int_{\operatorname{inside}(C)} |I(x) - c_1|^2 dx + \sigma_2 \int_{\operatorname{outside}(C)} |I(x) - c_2|^2 dx \right\}. \quad (3)$$

In our case, we set empirically $\mu = 0.2, \nu = 0, \sigma_1 = \sigma_2 = 0.8$. The minimization was accomplished by applying the level set technique, as described in Ref. 25, which, instead of manipulating C explicitly, represents it as the zero-crossing of a level set function. The level set function was initialized using the endocardial contour provided by the adaptive thresholding algorithm.

2.1.3 Endocardial boundary—region growing

The third segmentation algorithm consisted in standard region growing²⁷ using as seed pixel the barycenter of the segmentation

mask provided by the adaptive thresholding method. Pixels were progressively added to the growing region by scanning the 8-neighborhood of each boundary pixel and aggregating the pixels such that $|I - \langle I_R \rangle| \leq 4$ with I the pixel value and $\langle I_R \rangle$ the mean gray-level inside the growing region.

2.1.4 Epicardial boundary

Epicardial boundary extraction was performed through the following steps:

- Rough right-ventricle (RV) segmentation using pixel thresholding (gray level >100) with a connectivity constrain and a topographic argument (rightmost quadrant with respect to LV cavity).
- Morphological dilation of the LV endocardium mask using structuring elements with increasing sizes as long as the intersection between the dilated mask and the RV mask remained empty.
- Using the result of the dilated mask for initialization, epicardial boundary extraction by means of the “active contour without edge” method described above with the same energy function as for endocardium segmentation.

2.2 Validation Using an Open Access Database

We exploited an open access cine-MR database of the LV of 18 patients referred to Mondor University Hospital (Paris, France) for recent myocardial infarction. The database contains voxel data as well as two manual segmentations of each sequence of images that were validated from a clinical point of view.²⁸ Patients were examined on a 1.5 T MR (Magnetom Symphony, Siemens, Erlangen, Germany). The number of SA slices required to cover the entire LV ranged from 9 to 14. The number of frames acquired during the entire cardiac cycle ranged from 22 to 37 depending on heart rate. Images were sampled on a 100×100 matrix with a pixel size ranging from 1.45 to 2.08 mm and a slice thickness of 6 mm without interslice gap. Further technical details regarding image acquisition and segmentation are described in Refs. 7 and 28. Conventional manual segmentation of the LV cavity was performed by two independent and blinded expert cardiologists using the Analyze software package (Biomedical Imaging Resource, Mayo Clinic Foundation, Rochester, Minnesota). For each slice location, the experts manually overlaid the endocardial contours both at ED and ES times. During manual tracing, papillary muscles and LV trabeculae were included within the LV myocardium.

For each patient, the datasets corresponding to ED and ES were processed using the hybrid algorithm described in the previous section. All the computations were performed blind to the results of the manual segmentation. For each patient and each key frame (ED and ES), the similarity between hybrid and expert segmentations was assessed using the Dice overlapping metrics, the true positive and false negative volume fractions, and the average perpendicular distance. The concordance between EDVs and ESVs, EFs, and MMs provided by the hybrid segmentation and the average value of the corresponding measures over the two expert segmentations was evaluated using Lin's concordance correlation coefficient.

2.3 Clinical Validation

We conducted a retrospective study on a cohort of 29 patients that had already been exploited for prospective assessment of gated blood pool SPECT versus CMR.²⁹ Patients were aged 61 ± 14 years (range 34 to 87 years), 70% were male. All had clinical indications for CMR study to diagnose cardiac disease or as follow-up. Reasons for referral were coronary artery disease ($n = 15$), myocarditis ($n = 4$), arrhythmogenic right ventricular dysplasia ($n = 2$), constrictive pericarditis ($n = 2$), pulmonary hypertension ($n = 4$), scleroderma ($n = 1$), and adrenergic cardiomyopathy ($n = 1$). All subjects were recruited from inpatient and outpatient populations at Montpellier University Hospital between August 2008 and June 2009. The study was approved by the local ethics committee, and the requirement for individual informed consent was waived.

2.3.1 CMR data acquisition

CMR data were collected on a 1.5 T scanner (Magnetom Sonata; Siemens Medical Solutions, Erlangen, Germany) using breath-hold TrueFISP cine CMR.³⁰ Multiplane localizers identified the cardiac position and the usual cardiac imaging planes using a standard iterative scouting technique. Retrospective ECG-gated cine images were then acquired using a segmented steady-state precession sequence TrueFISP. About 10 to 25 SA views encompassing the entire LV and RV were acquired using the following parameters from the Society for Cardiovascular Magnetic Resonance (SCMR).³¹ Slice thickness was 6 to 13 mm with a 2-mm interslice gap, 256×208 matrix with a pixel size ranging from 1.48 to 2.29 mm, temporal resolution 40 ms, and field-of-view diameter of 30 to 40 cm depending on the patient's chest size.

2.3.2 CMR processing

Images were examined offline by an expert radiologist using commercially available software (ARGUS, Siemens Medical Solutions). LV contours were drawn on all phases and ES and ED were automatically defined as the phases with the highest and lowest volumes. CMR values were derived independently by modified Simpson's rule from semiautomated SA regions that were modified manually to conform to endocardial borders.^{32,33} Ventricular basal limits were defined as proposed by Alfakih et al.³⁴ In line with the SCMR recommendations, no corrections were performed to compensate for papillary muscles, so as to simplify the CMR measurements for optimal reproducibility, saving postprocessing time, and to use local institution normal reference ranges.^{31,35} In 15 patients for whom there was a suspicion of LV hypertrophy, the epicardial boundary was manually delineated on ED frame, which allowed the estimation of MM. Because LV epicardial delineation is a time-consuming operation, it was not systematically performed in patients without suspicion of LV hypertrophy.

CMR data were also processed using the automatic algorithm described in the previous section. For each patient, the first SA slice corresponding to the left ventricular basal limit was chosen by visual inspection with the help of coregistered long axis slices. All frames were systematically processed. ED and ES frames were defined as those corresponding to maximal and minimal LV volume, respectively. All the computations were performed blind to the results of the expert manual postprocessing. The concordance between EDVs and ESVs and EFs provided

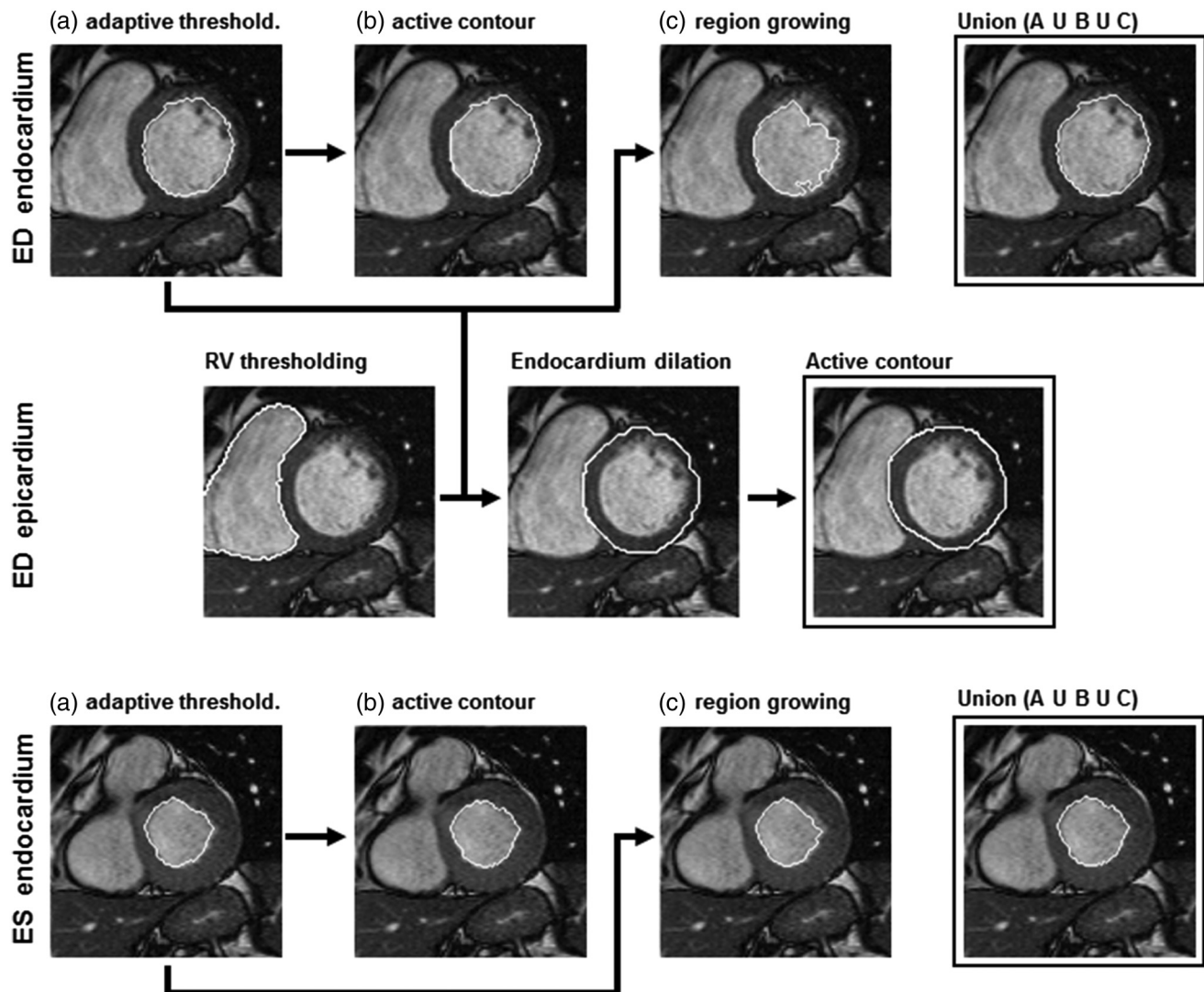


Fig. 1 Diagram of the steps of the hybrid segmentation. From top to bottom: ED endocardium, ED epicardium, and ES endocardium. Endocardial boundary was segmented using successively (a) adaptive thresholding, (b) active contour, and (c) region growing. Active contour and region growing used as input the result of adaptive thresholding. Final endocardial segmentation was the union of (a), (b), and (c). Epicardial boundary was segmented using dilation of the endocardial boundary and then active contour and was constrained by RV segmentation.

by the hybrid segmentation and the value of the corresponding measures provided by CMR manual segmentation was evaluated using Lin's concordance correlation coefficient and Bland-Altman analysis.

3 Results

The average processing time for one SA image was about 1 s including visual inspection of the segmented regions produced by Otsu's histogram clustering, mouse clicking that with the lowest intensity belonging to LV cavity, and the subsequent numerical computations for automatic endocardium and epicardium delineation. Accordingly, for a typical cine-MR study composed of 15 to 20 SA slices and 15 to 20 time frames, the total processing time using our hybrid method was about 5 min using an Intel® Core™ 2 Duo 2.20 GHz central processing unit with 2 Gb of RAM.

3.1 Validation Using an Open Access Database

Figure 1 schematizes the steps of the hybrid segmentation method for (from top to bottom) ED endocardium, ED epicardium, and ES endocardium. For illustration purposes, Fig. 2 shows the results provided by the hybrid method (top rows) and by expert manual delineation (middle and bottom rows) for patient #1 from the database (two more representative examples from the database are available at Ref. 36).

Figure 3 shows the results in terms of Dice overlapping metrics between hybrid and expert segmentations (light gray) and between the two expert segmentations (dark gray). Mean hybrid-expert similarity was 92.3% (versus 94.8% for mean interexpert similarity) regarding ED endocardial boundary, 88.4% (versus 92.1%) for ES endocardial boundary, and 91.5% (versus 96.2%) for ED epicardial boundary. Figure 4 shows the results in terms of average perpendicular distance (APD). Mean hybrid-expert APD was 1.6 mm (versus 1.1 mm for



Fig. 2 Results of the hybrid method and expert manual delineation for patient #1 from the open access database.

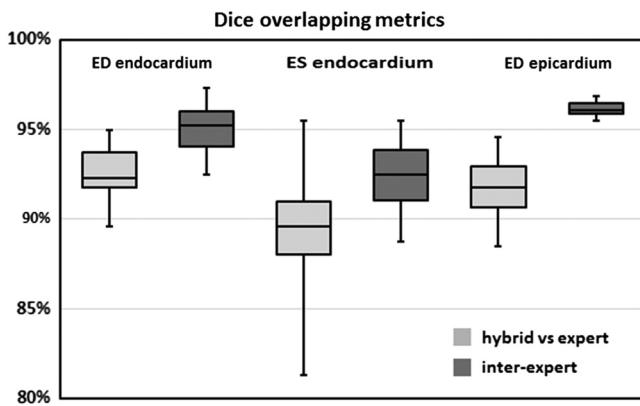


Fig. 3 Hybrid versus expert and interexpert similarity (Dice index) in LV contour delineation for ED and ES endocardium and ED epicardium. Boxes: median and interquartile range, whiskers: mean \pm 1.5 std dev.

mean interexpert APD) regarding ED endocardium, 1.9 mm (versus 1.3 mm) for ES endocardium, and 2.2 mm (versus 1.0 mm) for ED epicardium. True-positive volume fractions were $89\% \pm 3\%$, $88\% \pm 2\%$, and $87\% \pm 4\%$ for ED endocardium, ES endocardium, and ED epicardium, respectively. Corresponding false-negative volume fractions were $11\% \pm 3\%$, $12\% \pm 2\%$, and $13\% \pm 4\%$, respectively.

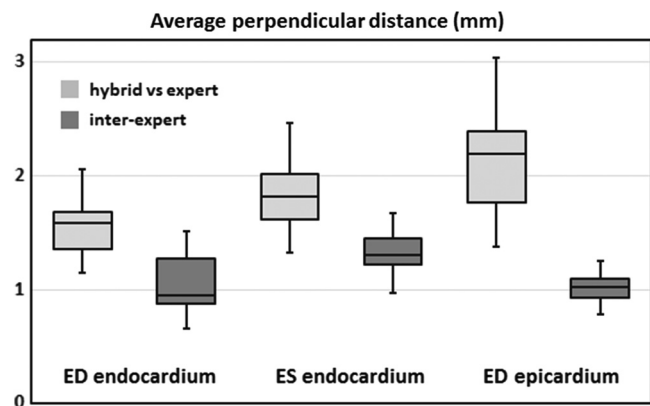


Fig. 4 Hybrid versus expert and interexpert average perpendicular distance in LV contour delineation for ED and ES endocardium and ED epicardium. Boxes: median and interquartile range, whiskers: mean \pm 1.5 std dev.

Table 1 summarizes the results of the comparison between hybrid and expert segmentations in terms of LV functional parameters. Concordance between hybrid and mean expert values as given by Lin's coefficient was good for ED volumes (0.91), ES volume (0.93), and EF (0.89). Concordance was lower yet fair regarding MM (0.74). The bias induced by hybrid segmentation with respect to mean expert values is to be

Table 1 Comparison between LV parameters given by expert manual delineation and hybrid semiautomated segmentation.

	Hybrid-expert concordance	Hybrid-expert bias	Interexpert concordance	Interexpert variability
ED volume (mL)	0.91	-11	0.94	5
ES volume (mL)	0.93	-4	0.93	6
Ejection fract. (%)	0.89	-3	0.91	4
MM (g)	0.74	-13	0.88	15

Note: ED: end-diastole, ES: end-systole, and MM: myocardial mass. All concordance coefficients are statistically significant ($p < 0.001$).

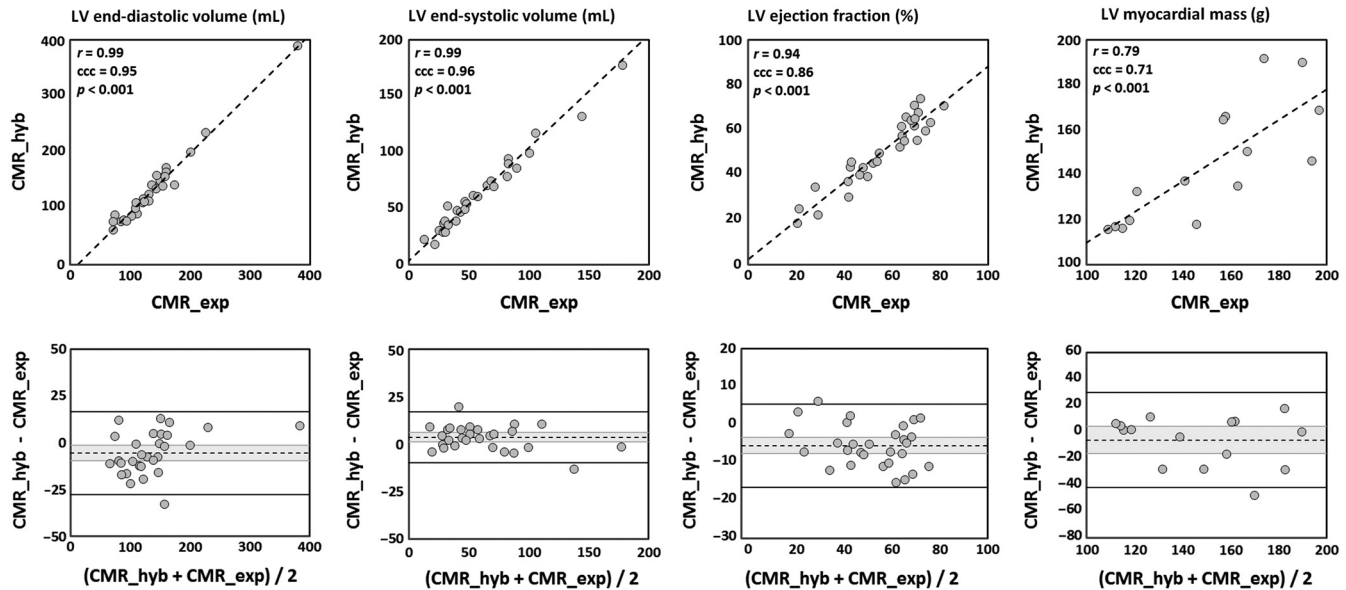


Fig. 5 Comparison between functional parameters (from left to right: LV EDV, LV ESV, LV EF, and LV mass) provided by hybrid segmentation (CMR_hyb) and manual expert segmentation (CMR_exp). Top: scatter plot. The dashed line stands for the linear regression (ccc: Lin's coefficient). Bottom: Bland-Altman diagram. The dashed lines indicate the mean difference (grayed is the 95% confidence interval) and the plain lines indicate the 95% limits of agreement.

compared with interexpert variability measured by root mean squared difference: -11 mL versus 5 mL for ED volume, -4 mL versus 6 mL for ES volume, -3% versus 4% for EF, and -13 g versus 15 g for MM.

3.2 Clinical Validation

Figure 5 shows the results regarding the comparison (correlation plot and Bland-Altman diagram) between LV functional parameters provided by the hybrid method and those given by manual expert segmentation (from left to right: LV EDV, LV ESV, LV EF, and LV mass). Concordance between hybrid and manual segmentation, as assessed by Lin's coefficient, was, respectively, 0.95, 0.96, and 0.86 for EDV, ESV, and EF (all p -values < 0.001). Regarding MM, there was a fair concordance between hybrid and expert estimations with a Pearson's correlation of 0.79 and a Lin's coefficient of 0.71 ($p < 0.001$). Compared to expert segmentation, hybrid segmentation underestimated EDVs (-6 mL, $p = 0.01$; 95% limits of agreement [-28 17] mL), overestimated ESVs (+4 mL, $p = 0.01$; [-10 17] mL), underestimated EFs (-6%, $p < 0.01$; [-17% 5%]), and underestimated MMs (-6 g, not significant; [-43 31] g).

4 Discussion

We described a hybrid method allowing for very fast and robust semiautomated extraction of LV endocardial and epicardial boundaries on cine-MR SA images. In clinical routine, expert radiologists or cardiologists are compelled to manually adjust on each SA slice a dozen of control points around the endocardial border and as much around the epicardial border, leading to a total processing time usually exceeding half an hour and final results that are naturally prone to intra- and interoperator variability. In view of the sustained increase in clinical demand for CMR examinations, along with the progressive reduction in acquisition time due to the development of fast imaging sequences, postprocessing quickness and robustness appear as crucial parameters, which will undoubtedly favor in the short to medium term a widespread diffusion of automated postprocessing tools in radiology labs.

The detailed results exposed in the previous section demonstrate that our hybrid method provides pertinent results in terms of LV functional parameters, which are perfectly compatible with routine clinical use. The assessment of the method using the 18 CMR open access database showed a fine similarity between hybrid and expert LV boundary delineations, with

a Dice overlapping index around 90% and a mean APD around 1.5 to 2 mm, versus ~95% and 1 to 1.5 mm for interexpert similarity. As a consequence, the hybrid–expert concordance for the derived clinical parameters was excellent, with a hybrid–expert bias that remained comparable to interexpert variability. The clinical validation on a retrospective cohort of 29 patients with various cardiomyopathies revealed once again an almost perfect concordance between hybrid and expert LV volumes and EFs. Hybrid–expert systematic bias, although statistically significant, was small compared to the required accuracy for clinical diagnosis and follow-up (<10 mL for LV volumes, –6% for EF). With respect to MM evaluated in a subgroup of 15 patients, hybrid–expert concordance was satisfying and systematic bias (<10 g) was neither clinically nor statistically significant.

The main limitation of our study is the lack of comparison with conventional semiautomated segmentation. This was due to the fact that such semiautomated segmentation results were not provided with the open access database. Semiautomated results were not available for patient data, because the radiology team in our institution do not use semiautomated software for routine LV assessment.

The results exposed here seem consistent with those reported previously using state-of-the-art semiautomated extraction techniques. In a systematic review of CMR segmentation methods, Petitjean and Dacher³ reported mean APDs to the reference segmentation ranging roughly from 1 to 2.5 mm for endocardium and 1 to 3 mm for epicardium. In more recent research, Zhang et al.¹⁷ used a combination of active shape model and active appearance model to produce a four-dimensional mesh of LV and RV. Resulting mean overlapping indices with the reference segmentation in normal subjects was 90% for LV endocardium and 92% for LV epicardium, corresponding to mean APDs of 1.7 and 1.8 mm, respectively. Ma et al.²³ proposed a neural network approach for gradient-based endocardium extraction coupled with a gradient vector flow snake for epicardium segmentation. In a mixed population of healthy and pathological subjects, the method yielded mean overlapping indices with the reference segmentation of 89% for endocardium and 92% for epicardium, both corresponding to APDs of 2.4 mm. Mean biases in EF and MM estimations were, respectively, 3% and 11 g, similar to those reported here. The foremost strengths of the hybrid method described in the present paper include a short processing time with minimal operator intervention, no prior regarding LV shape or signal distribution, both endocardial and epicardial boundary extraction, high similarity with expert manual delineation yielding low bias in LV parameters estimation with respect to interexpert variability, and full clinical validation against classical CMR in terms of LV volume, EF, and MM, in a population of patients with various cardiomyopathies. Further development is ongoing to improve the technique toward full automation of LV cavity localization using Hough's transform and motion tracking between adjacent slices and time frames.

5 Conclusion

This paper presents an original semiautomated algorithm for LV segmentation, which allows both endocardium and epicardium extraction in a short processing time with minimal operator intervention. Its evaluation using an open access database showed a high similarity of the produced contours with those provided by expert manual delineation. The validation study conducted on a cohort of patients demonstrated that its results

in terms of LV parameters (volume, EF, and MM) were concordant with those obtained by expert postprocessing, which attests that the method should be workable in daily clinical practice.

Disclosures

The authors have no relevant financial interests in this manuscript.

References

1. A. Suinesiaputra et al., "Quantification of LV function and mass by cardiovascular magnetic resonance: multi-center variability and consensus contours," *J. Cardiovasc. Magn. Reson.* **17**, 63 (2015).
2. J. Anderson et al., "Normal cardiac magnetic resonance measurements and interobserver discrepancies in volumes and mass using the papillary muscle inclusion method," *Open Gen. Intern. Med. J.* **1**, 6–12 (2007).
3. C. Petitjean and J. Dacher, "A review of segmentation methods in short axis cardiac MR images," *Med. Image Anal.* **15**, 169–184 (2011).
4. P. Peng et al., "A review of heart chamber segmentation for structural and functional analysis using cardiac magnetic resonance imaging," *MAGMA* **29**(2), 155–195 (2016).
5. A. Goshtasby and D. Turner, "Segmentation of cardiac cine MR images for extraction of right and left ventricular chambers," *IEEE Trans. Med. Imaging* **14**, 56–64 (1995).
6. E. Natchomy et al., "Automatic assessment of cardiac function from short-axis MRI: procedure and clinical evaluation," *Magn. Reson. Imaging* **16**, 365–376 (1998).
7. J. Cousty et al., "Segmentation of 4D cardiac MRI: automated method based on spatiotemporal watershed cuts," *Image Vision Comput.* **28**, 1229–1243 (2010).
8. J. Yeh et al., "Myocardial border detection by branch-and-bound dynamic programming in magnetic resonance images," *Comput. Methods Programs Biomed.* **79**, 19–29 (2005).
9. A. Pednekar et al., "Automated left ventricular segmentation in cardiac MRI," *IEEE Trans. Biomed. Eng.* **53**, 1425–1428 (2006).
10. M. Lynch, O. Ghita, and P. Whelan, "Automatic segmentation of the left ventricle cavity and myocardium in MRI data," *Comput. Biol. Med.* **36**, 389–407 (2006).
11. M. R. Rezaee et al., "A multi-resolution image segmentation technique based on pyramidal segmentation and fuzzy clustering," *IEEE Trans. Image Process.* **9**, 1238–1248 (2000).
12. I. B. Ayed, S. Li, and I. Ross, "Embedding overlap priors in variational left ventricle tracking," *IEEE Trans. Med. Imaging* **28**, 1902–1913 (2009).
13. H. Y. Lee et al., "Automatic left ventricle segmentation using iterative thresholding and an active contour model with adaptation on short-axis cardiac MRI," *IEEE Trans. Biomed. Eng.* **57**(4), 905–913 (2010).
14. J. Sénégas, C. Cocosco, and T. Netsch, "Model-based segmentation of cardiac MRI cine sequences: a Bayesian formulation," *Proc. SPIE* **5370**, 432–443 (2004).
15. M. Lynch, O. Ghita, and P. Whelan, "Left-ventricle myocardium segmentation using a coupled level-set with a priori knowledge," *Comput. Med. Imaging Graphics* **30**, 255–262 (2006).
16. N. Paragios, "A level set approach for shape-driven segmentation and tracking of the left ventricle," *IEEE Trans. Med. Imaging* **22**, 773–776 (2003).
17. H. Zhang et al., "4-D cardiac MR image analysis: left and right ventricular morphology and function," *IEEE Trans. Med. Imaging* **29**, 350–364 (2010).
18. S. Mitchell et al., "Multistage hybrid active appearance model matching: segmentation of left and right ventricles in cardiac MR images," *IEEE Trans. Med. Imaging* **20**, 415–423 (2001).
19. J. Lötjönen et al., "Statistical shape model of atria, ventricles and epicardium from short- and long-axis MR images," *Med. Image Anal.* **8**, 371–386 (2004).
20. M. Lorenzo-Valdés et al., "Segmentation of 4D cardiac MR images using a probabilistic atlas and the EM algorithm," *Med. Image Anal.* **8**, 255–265 (2004).
21. P. Balzer et al., "Simultaneous and correlated detection of endocardial and epicardial borders on short-axis MR images for the measurement of left ventricular mass," *Radiographics* **18**, 1009–1018 (1998).

22. C. Corsi et al., "Improved quantification of left ventricular volumes and mass based on endocardial and epicardial surface detection from cardiac MR images using level set models," *J. Cardiovasc. Magn. Reson.* **7**, 595–602 (2005).
23. Y. Ma et al., "An SPCNN-GVF-based approach for the automatic segmentation of left ventricle in cardiac cine MR images," *Int. J. Comput. Assist. Radiol. Surg.* **11**, 1951–1964 (2016).
24. N. Otsu, "A threshold selection method from gray-level histograms," *IEEE Trans. Syst. Man Cybern.* **9**, 62–66 (1979).
25. T. Chan and L. Vese, "Active contours without edges," *IEEE Trans. Image Process.* **10**, 266–277 (2001).
26. D. Mumford and J. Shah, "Optimal approximation by piecewise smooth functions and associated variational problems," *Commun. Pure Appl. Math.* **42**, 577–685 (1989).
27. W. K. Pratt, *Digital Image Processing*, 4th ed., John Wiley & Sons, Inc., Los Altos, California (2007).
28. L. Najman et al., "An open, clinically-validated database of 3D+t cine-MR images of the left ventricle with associated manual and automated segmentations," in Insight Journal, *Special Issue Entitled ISC/NA-MIC Workshop on Open Science at MICCAI* (2007).
29. L. Sibille et al., "Comparative values of gated blood-pool SPECT and CMR for ejection fraction and volume estimation," *Nucl. Med. Commun.* **32**, 121–128 (2011).
30. J. C. Carr et al., "Cine MR angiography of the heart with segmented true fast imaging with steady-state precession," *Radiology* **219**, 828–834 (2001).
31. C. M. Kramer et al., "Standardized cardiovascular magnetic resonance imaging (CMR) protocols, society for cardiovascular magnetic resonance: board of trustees task force on standardized protocols," *J. Cardiovasc. Magn. Reson.* **10**, 35 (2008).
32. H. Thiele et al., "Improved accuracy of quantitative assessment of left ventricular volume and ejection fraction by geometric models with steady-state free precession," *J. Cardiovasc. Magn. Reson.* **4**, 327–339 (2002).
33. M. C. Dulce et al., "Quantification of the left ventricular volumes and function with cine MR imaging: comparison of geometric models with three-dimensional data," *Radiology* **188**, 371–376 (1993).
34. K. Alfakih et al., "Assessment of ventricular function and mass by cardiac magnetic resonance imaging," *Eur. Radiol.* **14**, 1813–1822 (2004).
35. B. Sievers et al., "Impact of papillary muscles in ventricular volume and ejection fraction assessment by cardiovascular magnetic resonance," *J. Cardiovasc. Magn. Reson.* **6**, 9–16 (2004).
36. M. Messadi and F. B. Bouallègue, "Supplementary examples of LV segmentation," https://scinti.edu.umontpellier.fr/files/2017/11/JMI_supplementary_examples.pdf (2018).

Mahammed Messadi is an associate professor in the Department of Biomedical Engineering at Tlemcen University, Algeria. He received an engineer degree in electronics in 2002 from Electronics Department of Technology Faculty. He also received his PhD in biomedical engineering from Tlemcen University in 2010. His research interests include image analysis with an emphasis on medical image preprocessing, feature extraction, and classification methods.

Abdelhafid Bessaid is a professor at Tlemcen University, Algeria. He received his diploma EL-Ing degree from the University of Science and Technology of Oran, Algeria, his master's and PhD degrees from the University of Sidi Bel Abbes, Algeria, in 1981, 1997, and 2004, respectively. He works since 1996 in the field of medical image processing at University of Tlemcen, Algeria.

Denis Mariano-Goulart received his engineering degree in physics from the Ecole Nationale Supérieure de physique, Marseille, France and his PhD in mathematical morphology from the Ecole Nationale Supérieure des Mines, Paris. He also graduated from Montpellier University as medical doctor. He is now a professor at Montpellier University and head of Nuclear Medicine Department at Montpellier University Hospital. His research interests include tomography and medical image analysis.

Fayçal Ben Bouallègue received his engineering degree in physics from the University of Liège, Belgium and his PhD in applied mathematics from Montpellier Science University, France. He also graduated from Montpellier University as medical doctor. He is currently working as a nuclear doctor at Montpellier University Hospital, as well as research and teaching assistant at Montpellier University. His research interests include tomography and medical image analysis.